Supporting information

Hybrid PDI/BiOCl composites with enhanced interfacial carriers transport for full-spectrum photocatalytic degradation pollutants

Xiaoming Gao[1], Kailong Gao[1], Xibao Li[2], Yanyan Shang[1], Feng Fu[1]

[1]Department of Chemistry and Chemical Engineering, Shaanxi Key Laboratory of Chemical Reaction Engineering, Yan'an University, Yanan, 716000, P. R.China

[2]School of Materials Science and Engineering, Nanchang Hangkong University, Nanchang 330063, P. R. China

Figures

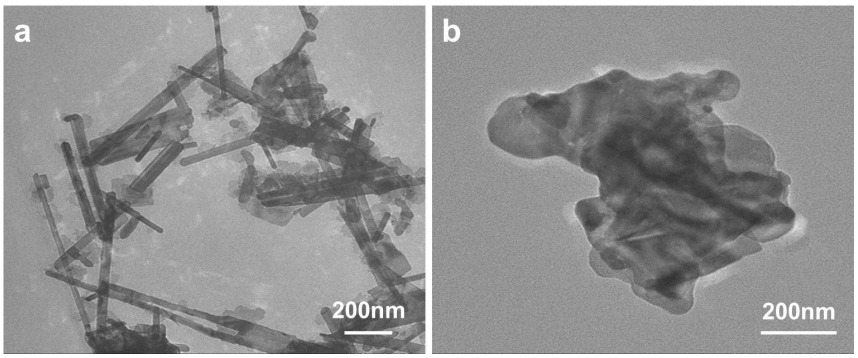

Fig. S1. (a) TEM images of BiOCl, (b) TEM images of PDI_{SA}

As shown in Fig. S1a, the prepared BiOCl had a long rod-like structure, and the length ranged from 50nm to 2um and cross-section of 5nm. As shown in Fig. S1b, the self-assembled PDI presented an irregular sheet structure.

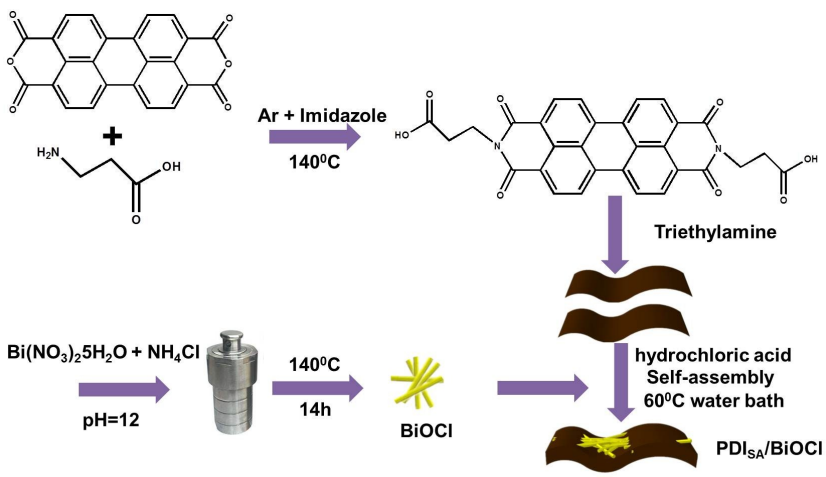

Fig. S2. The growth scheme of BiOCl/PDI

According to the analysis of TEM, the construction process of BiOCl/PDI could be assumed as Fig. S2. PDI was formed by reaction of PDTA and β-alanine at 140℃ under argon protection. Under acidic conditions, PDI could self-assemble by hydrogen bonding and stacking of π-π bond. In this way, the band structure for the transition of photogenerated electron was formed. Meanwhile, rod-like BiOCl was formed with $Bi(NO_3)_2$ and NH_4Cl by hydrothermal method. During the preparation of BiOCl/PDI, BiOCl was added and participated in the self-assembly of PDI, which expanded the light-harvesting range of BiOCl and improved the thermal stability of PDI.

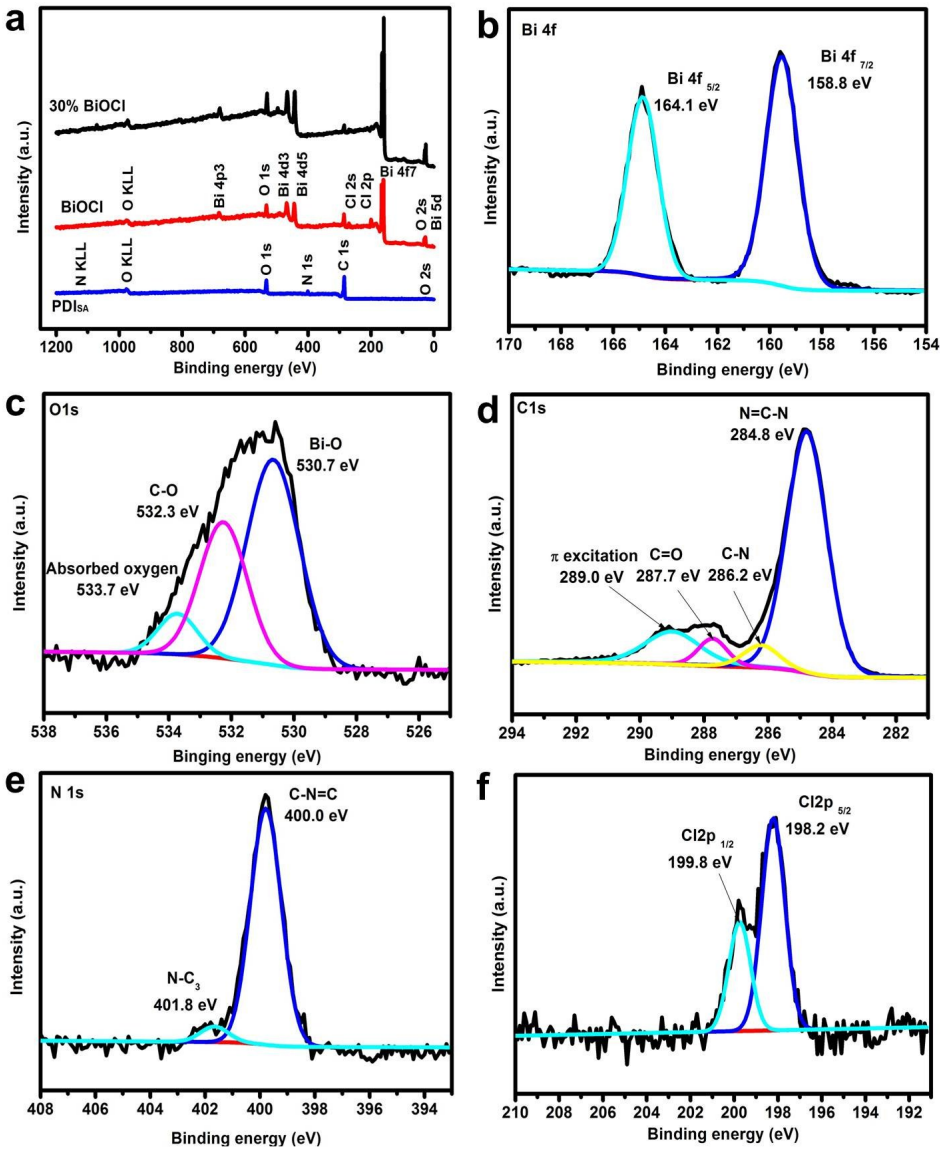

Fig. S3. (a) XPS survey spectra of BiOCl, PDI_{SA} and 30% BiOCl; HR-XPS spectra of (b) Bi, (c) O, (d) C (e) N and (f) Cl of 30% BiOCl

From the full spectrum of XPS (Fig. S3a), PDI/BiOCl was composed of Bi, O, Cl, C and N elements, which proved that BiOCl participated in the self-assembly of PDI. As shown in Bi4f spectrum (Fig. S3b), two peaks at 158.8 eV and 164.1 eV can be assigned to $Bi4f_{7/2}$ and $Bi4f_{5/2}$, respectively. From Fig. S3c, three peaks were located at 530.7 eV, 532.3 eV and 533.7 eV, which could be ascribed to two types of oxygen. The one type was lattice oxygen with Bi-O and C-O bonds. The main peak at 530.7 eV corresponded to Bi-O bond in BiOCl. The peak at 532.3 eV belonged to C-O bond in PDI. The other type at 533.7 eV belonged to O-H bond or O-O bond of absorbed H_2O or O_2. In Fig. S3d, there were four peaks at 284.8 eV, 286.2 eV, 287.7 eV and 289.0 eV. The main peak at 284.8 eV belonged to sp_2 hybrid carbon, which corresponded to N = C-N.

The peak at 286.2 eV corresponded to C-N, and the peak at 287.7 eV belonged to C = O. However the peak at 289.0 eV belonged to π electron excitation, indicating the self-assembly structure of π-π* stacking. In HR-XPS spectrum of N element (Fig. S3e), there were two characteristic peaks at 400.0 eV and 401.8 eV. The peak at 400.0 eV belonged to sp_2 hybrid nitrogen, which could be ascribed to C-N=C. Moreover, the peak at 401.8 eV belonged to N-C_3. In Fig. S3f, the peaks of Cl $2p_{1/2}$ and Cl $2p5_{/2}$ was located at 199.8 eV and 198.2 eV.

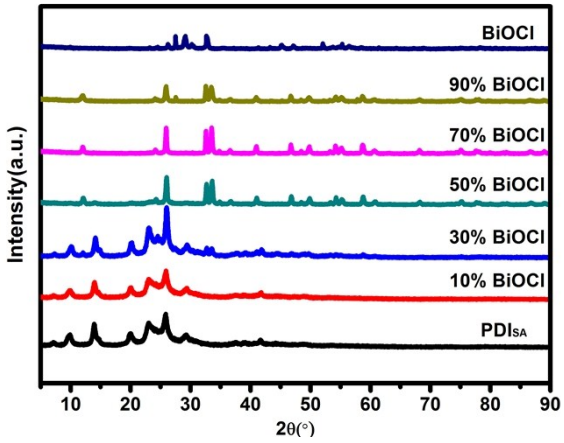

Fig. S4. XRD patterns of as-prepared samples

From Fig. **S4**, there were diffraction peaks at 2θ = 10.1°, 14.2°, 19.7, 22.8°, 25.8° in the XRD patterns of PDI_{SA}. The characteristic diffraction peaks of BiOCl were not obvious when the amount of BiOCl was small. The intensity of diffraction peak of PDI_{SA} increased with the increase of BiOCl amount (less than 30%), indicating that BiOCl could strength the self-assembly of PDI. However, when the BiOCl amount was more than 30%, the intensity of diffraction peak of PDI_{SA} decreased with the increasing of BiOCl, but the diffraction peak at 2θ = 25.8° still existed, indicating the existence of self-assembly structure in PDI. This might be due to the poor crystallinity of PDI_{SA}, which interfered with the detection of diffraction peak of PDI. Moreover, the intensity of diffraction peak of 30% PDI/BiOCl at 2θ = 25.8° was strengthen, which indicated it was of strong π-π stacking function. When BiOCl amount was more than 30%, the characteristic diffraction peaks of BiOCl (PDF No. 00-006-0246) began to appear at 2θ = 33.8°. With the increasing of BiOCl, the other characteristic diffraction peaks were obvious and the intensity was enhanced. These phenomena implied that BiOCl particles were involved in the self-assembly of PDI.

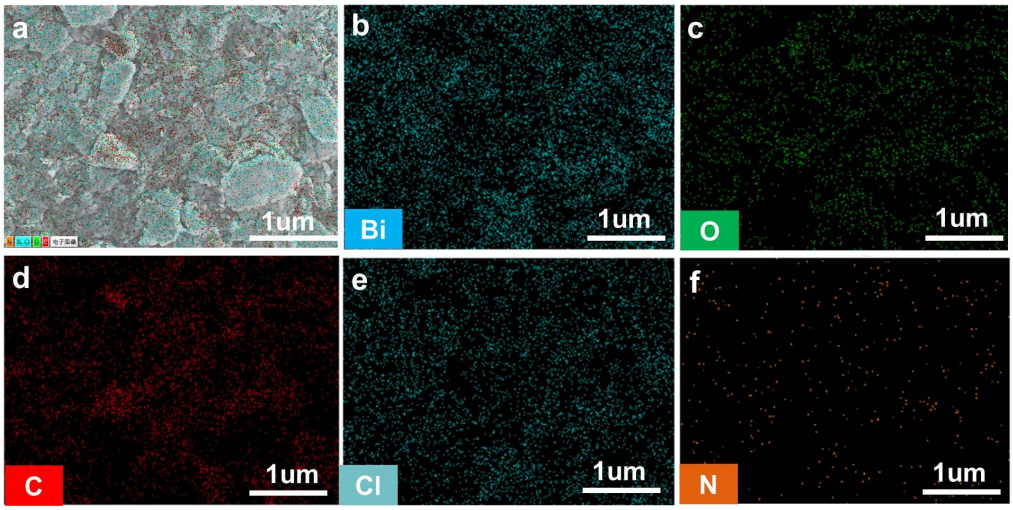

Fig. S5. (a) EDS mapping of element distribution of 30% BiOCl, (b) Bi, (c) O, (d)C, (e) Cl and (f) N distribution

As shown in the EDS of 30% BiOCl (Fig. **S5**), Bi, O, Cl, C and N elements were uniformly distributed on the surface of the sample, and the distribution area was consistent with the SEM, and no other elements existed.

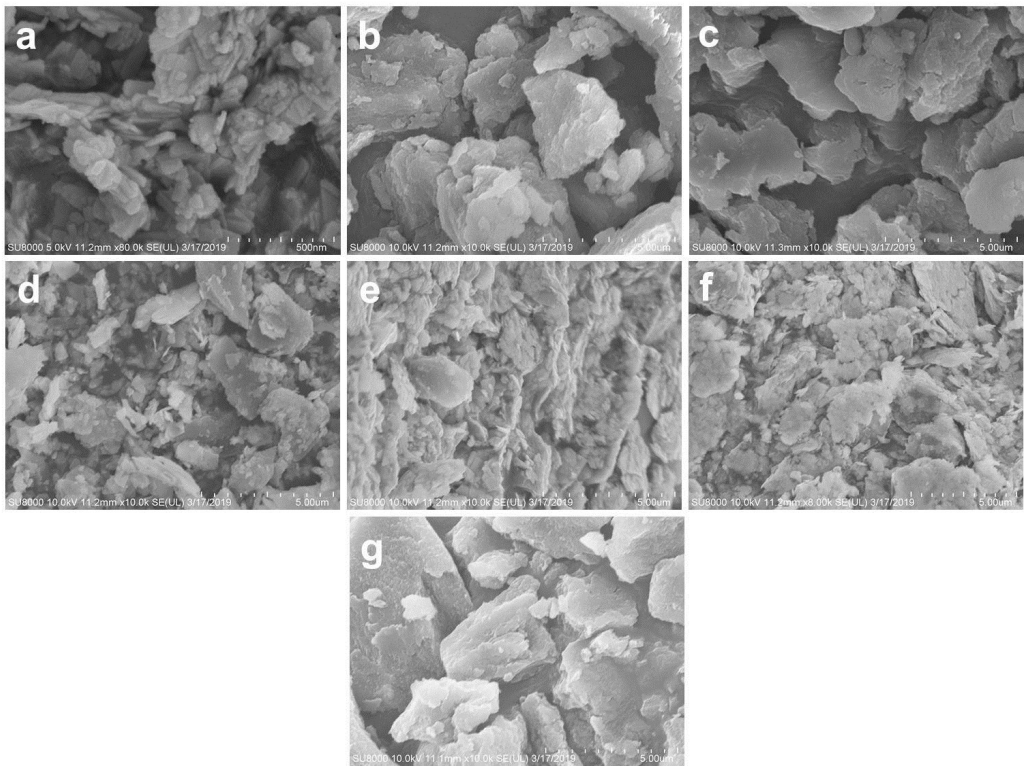

Fig. S6. SEM images of the as-prepared samples (a) BiOCl, (b) 10% BiOCl, (c) 30% BiOCl, (d) 50% BiOCl, (e) 70% BiOCl, (f) 90% BiOCl and (g) PDI_{SA}

The SEM of BiOCl, PDISA and PDI/BiOCl are shown in Fig. **S6**. As shown in Fig. **S6**a, BiOCl was rod-like structure. From Fig. **S6**g, PDI_{SA} was a polymer with sheet-like structure formed by self-assembly of PDI monomers under acidic conditions. When the self-assembly environment of PDI was single and no influence of other media, a large number of PDI self-assembled rapidly under the action of hydrogen bond and π-π* stacking. Afterwards, the polymers were formed with small entropy energy, stable structure and larger shape under the thermodynamics. With the addition of BiOCl, the shape of PDI_{SA} polymer decreased. The reason was probably the change of self-assembly environment owing to the participation of BiOCl, which slowed down the self-assembly speed, thus formed smaller aggregates. With the increase of BiOCl addition, the polymer decreaseed further. Especially, as the BiOCl addition was 90% (Fig. **S6**f), the polymer with flake PDI_{SA} and rod BiOCl could be observed obviously.

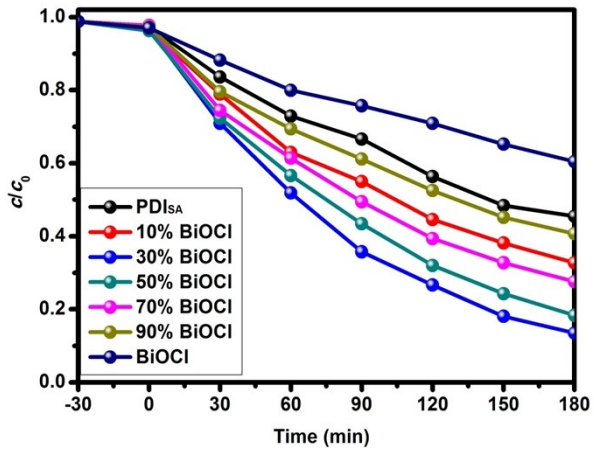

Fig. S7. The full spectrum photocatalytic activity of as-prepared samples

From Fig. **S7**, the removal rates of phenol by BiOCl and PDI_{SA} were respectively higher than that of PDI/BiOCl after 180 min illumination, which confirmed that the hybrid phase interface favored in the efficient carriers transfer, which could improve the photocatalytic degradation activity. With the increase of BiOCl amount, the photocatalytic activity of PDI/BiOCl increased, and then decreased.

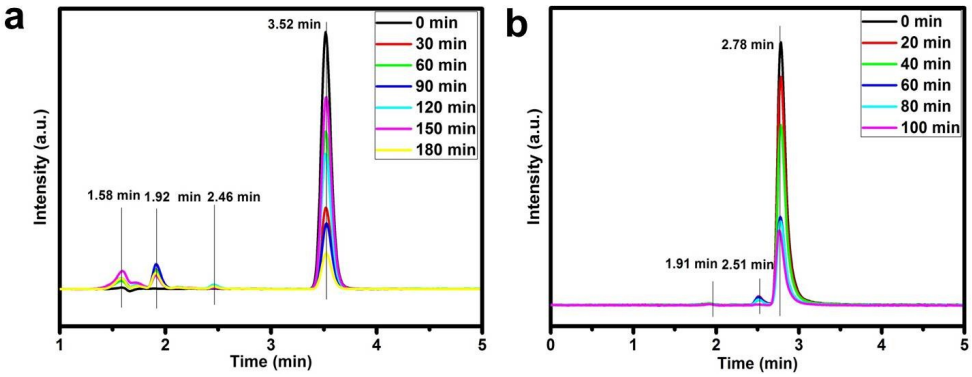

Fig. S8. HPLC spectrum of phenol(a) and MB(b) degradation at different reaction time over 30% BiOCl under full spectrum irradiation

The intermediate products of full spectrum photocatalytic degradation of phenol by 30% BiOCl were analyzed by high performance liquid chromatography (HPLC), and the results are shown in Fig. **S8**a. From Fig. **S8**a, there was main peak at 3.52 min of retention time, which corresponded to phenol. With the prolonging of illumination time, the peak intensity at 3.52 min decreased gradually, indicating that phenol was degraded and converted during the photocatalytic degradation. Meanwhile, there were three main peaks with 1.58 min, 1.92 min and 2.46 min of retention time, which could be assigned to the intermediate degradation products of phenol of hydroquinone, p-benzoquinone and catechol. With the photocatalytic reaction, the peak of hydroquinone, p-benzoquinone and catechol gradually increased, and then decreased. The retention peak of hydroquinone was strongest at 150 min. The peak of p-benzoquinone gradually increased and then weakened at 30-90 min. However, the peak of catechol gradually increased and then weakened at 30-120 min. Therefore, the benzene ring could be destroyed and converted into small molecular organic acids over PDI/BiOCl. In order to confirm the degradation activity of PDI/BiOCl for organic pollutants, the intermediate products of photocatalytic degradation of MB by 30% BiOCl were analyzed by HPLC, and the results are shown in Fig. **S8**b. From Fig. **S8**b, the main peaks were located at 1.91 min, 2.51 min and 2.78 min of retention time. The peak of 2.78 min of retention time corresponded to MB. With the prolonging of illumination time, the peak intensity gradually decreased, indicating that MB was degraded and converted. The peaks located at 1.91 min and 2.51 min of retention time corresponded to the intermediate degradation products of MB. The peaks could be observed in the former stage of photocatalytic degradation, with the photocatalytic reaction, the peak of intermediate products gradually decreased, and the peak nearly

disappeared at 100 min. It indicated that 30% BiOCl could mineralize MB into small molecules under the light illumination, such as small organic acids, CO_2 and H_2O.

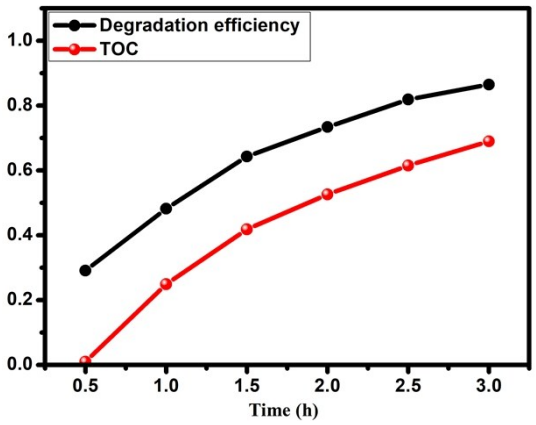

Fig. S9. Photocatalytic removal effect of TOC and phenol over 30% BiOCl.

The full spectrum photocatalytic degradation of phenol was investigated by total organic carbon (TOC) analyzer. As shown in Fig. S9, the degradation rate of 30% BiOCl has been obtained 80.7%, while the mineralization rate of phenol was about 69.2% during 180 min.

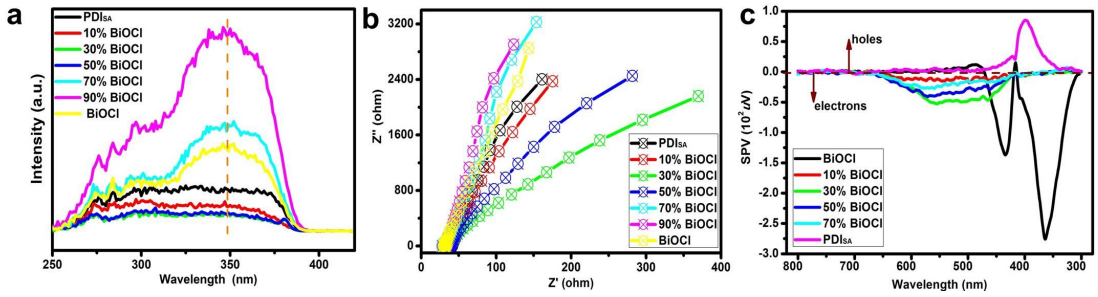

Fig. S10 (a) Photo-luminescence (PL) spectra with excitation wavelength of 220nm, (b) Nyqiust plots with 300W xenon lamp, (c) Surface photovoltage spectrum of the as-prepared samples

PL spectra could be used to measure the separation efficiency of photogenerated carriers. The higher PL intensity implied the lower separation efficiency of electron-hole pairs. Fig. S10a shows that 30% BiOCl had lower PL peak, indicating 30% BiOCl had higher separation efficiency of photogenerated carriers. The combination of BiOCl and PDI_{SA} could effectively inhibit the recombination of photogenerated carriers and improved the photocatalytic performance. The electrochemical impedance spectroscopy of the sample is shown in Fig. S10b. The arc radius of the Nyqiust curve of 30% BiOCl was obviously smaller, indicating that the charge transfer resistance of 30% BiOCl was smaller, and the charge transfer efficiency was improved. In the irradiated light of 300 nm - 800 nm, BiOCl presents negative SPV signal, nevertheless PDI_{SA} appeared positive SPV signal (Fig. S10c). It demonstrated that the main carriers of BiOCl were photogenerated electrons, and the photogenerated holes for PDI_{SA}. When the hybrid PDI/BiOCl composites were formed, under the light irradiation, the photoinduced electrons were injected into BiOCl from PDI, and the photogenerated holes were accumulated in PDI. In addition, 30% BiOCl showed stronger SPV signal than that of the other PDI/BiOCl composites, which could be ascribed to the different interfacial interaction between the BiOCl and PDI.

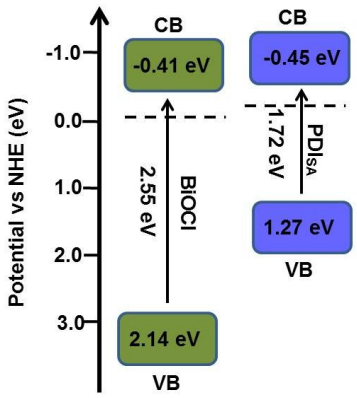

Fig. S11. Band alignment structure of PDI_{SA} and BiOCl

E_{VB} of BiOCl and PDI_{SA} could be estimated to 2.14 eV and 1.27 eV. Because the conduction band energy of PDI_{SA} was more negative than that of BiOCl, and the valence band energy of BiOCl was more positive than that of PDI_{SA} (Fig. **S11**), direction Z-scheme heterojunction was constructed by PDI_{SA} and BiOCl, which not only increased the quantity of carriers, but also extended transmission path of carriers. The photocatalytic activity was improved by isolating and inhibiting the recombination of the photogenerated carriers.

Tables

Table S1 Atomic content of PDI/BiOCl analyzed by XPS

samples	C	N	O	Cl	Bi
BiOCl	36.64	/	39.02	2.62	21.72
10% BiOCl	73.57	4.93	21.15	0.24	0.11
50% BiOCl	57.03	3.16	23.27	7.60	8.93
PDI	77.77	3.59	18.64	/	/

The atomic content of PDI/BiOCl was analyzed by X-ray photoelectron spectroscopy (XPS). It demonstrated that the heterojunction BiOCl/PDI was constructed. As for the C content, there was often a large deviation for the results of XPS, so we did not discuss it here.